Hindawi Publishing Corporation
Journal of Applied Mathematics
Volume 2012, Article ID 738082, 21 pages
doi:10.1155/2012/738082

Research Article

Analysis of Mechanical Energy Transport on Free-Falling Wedge during Water-Entry Phase

Wen-Hua Wang,[1,2] Yi Huang,[2,3] and Yan-Ying Wang[3]

[1] *State Key Laboratory of Structural Analysis for Industrial Equipment, Dalian University of Technology, Dalian 116024, China*
[2] *Deepwater Engineering Research Center, Dalian University of Technology, Dalian 116024, China*
[3] *School of Naval Architecture, Dalian University of Technology, Dalian 116024, China*

Correspondence should be addressed to Wen-Hua Wang, wangwenhua0411@yahoo.cn

Received 19 January 2012; Accepted 25 March 2012

Academic Editor: Di Liu

For better discussing and understanding the physical phenomena and body-fluid interaction of water-entry problem, here mechanical-energy transport (wedge, fluid, and each other) of water-entry model for free falling wedge is studied by numerical method based on free surface capturing method and Cartesian cut cell mesh. In this method, incompressible Euler equations for a variable density fluid are numerically calculated by the finite volume method. Then artificial compressibility method, dual-time stepping technique, and Roe's approximate Riemann solver are applied in the numerical scheme. Furthermore, the projection method of momentum equations and exact Riemann solution are used to calculate the fluid pressure on solid boundary. On this basis, during water-entry phase of the free-falling wedge, macroscopic energy conversion of overall body-fluid system and microscopic energy transformation in fluid field are analyzed and discussed. Finally, based on test cases, many useful conclusions about mechanical energy transport for water entry problem are made and presented.

1. Introduction

Water-entry phenomena are very common and important in many practical projects, so it is clear that researches on various water-entry models are always the focus in the field of ship and ocean engineering. For better discussing and understanding the physical phenomena and body-fluid interaction during water-entry phase, this paper mainly discusses and studies the mechanical energy transport from two aspects, which are macroscopic energy conversion of overall wedge-fluid system and microscopic energy transformation in fluid field, respectively.

However, it is a hard task for water-entry problem to deal with moving free surface and solid boundary simultaneously. Furthermore, the body-fluid interaction during water

impact should increase the difficulty and complexity of accuracy calculation as discussed by Bunnik and Buchner [3]. Thus here an effective and available numerical method based on free surface capturing method and Cartesian cut cell mesh as studied by W. H. Wang and Y. Y. Wang [4] can be used to well handle the difficulty of moving free surface and solid boundary.

In this numerical method, by using free surface capturing method as discussed in [4–7], the incompressible Euler equations for a variable density fluid are taken as governing equations, and free surface should be captured as a contact discontinuity in the density field. On the other hand, Owing to its advantage of conveniently updating a few cells locally near solid boundary rather than remeshing the whole flow domain, Cartesian cut cell mesh system as shown [8–10] is applied to treat the moving body. Then, finite volume method is used to numerically discretize governing equations. In the numerical method, Roe's approximate Riemann solver as discussed by Roe [11] is introduced for flux evaluation at each edge of fluid cell, and the exact Riemann discontinuous solution as studied by W. H. Wang and Y. Y. Wang [4] is taken to achieve the flux on the solid boundary. Besides, dual-time stepping technique with artificial compressibility method as discussed by Soh and Goodrich [12] is applied in time advancing. Furthermore, the body-fluid interaction is calculated by means of a fully body-fluid coupled method as described by Kelecy and Pletcher [13].

On this basis, the theory of energy transport as demonstrated by Bird et al. [14] is introduced in the water-entry model to analyze and discuss the regularity about macroscopic energy conversion of overall wedge-fluid system and microscopic energy transformation in fluid field during water-entry phase. Finally, by taking water-entry model of free-falling wedge as test cases, many useful conclusions about mechanical energy transport for water-entry problem are made and presented.

2. Numerical Computational Method for Water-Entry Model

2.1. Governing Equations and Boundary Condition

Here, free surface capturing method is applied to treat water surface. For the 2D incompressible, unsteady, inviscid fluid system with a variable density field, the fixed x- and y-coordinate axes are along and vertical to free surface, respectively, so the governing equations can be written in the conservation form as follows.

The mass conservation equation:

$$\frac{\partial \rho}{\partial t} + \frac{\partial (\rho u)}{\partial x} + \frac{\partial (\rho v)}{\partial y} = 0, \tag{2.1}$$

the x-direction momentum equation:

$$\frac{\partial (\rho u)}{\partial t} + \frac{\partial (\rho u u + p)}{\partial x} + \frac{\partial (\rho u v)}{\partial y} = \rho B_x, \tag{2.2}$$

the y-direction momentum equation:

$$\frac{\partial(\rho v)}{\partial t} + \frac{\partial(\rho v u)}{\partial x} + \frac{\partial(\rho v v + p)}{\partial y} = \rho B_y, \tag{2.3}$$

and the incompressibility constraint equation:

$$\frac{\partial u}{\partial x} + \frac{\partial v}{\partial y} = 0, \tag{2.4}$$

where ρ is the fluid density, u, v represent the x- and y-directional fluid velocities, p is the fluid pressure, and B_x and B_y are the x and y-directional accelerations of body force, respectively.

In the current method, two kinds of boundary conditions should be used and described as

(1) outlet or open boundary: a zero gradient condition is applied to the velocity and density, and the pressure at this boundary is fixed to be static pressure, which allows fluid to enter or leave the computational domain freely according to the local flow velocity and direction;

(2) solid body boundary: the density is assumed to have a zero normal gradient, and the no-penetration condition can be applied to the velocity. For the case that a free rigid body moves with one degree (up or down) by referring to W. H. Wang and Y. Y. Wang [4], the projection method for momentum (2.2)-(2.3) is used to define the pressure boundary condition $\nabla p = [0, -\rho \partial v_S / \partial t - \rho g]$, here v_S^n is the vertical velocity of free-falling wedge with positive direction upwards.

2.2. Cartesian Cut Cell Mesh System

In the present study, Cartesian cut cell mesh is applied in spatial discretization of computational domain, which can be generated by cutting solid bodies out of a background Cartesian mesh. As a result, three kinds of cells (solid, fluid, and cut cell) are formed, in which geometric and fluid information can be stored. Moreover, the further detail about the mesh generation can be referred to the studies of Yang et al. [8, 9] and Causon et al. [10].

2.3. Numerical Discretization Scheme

Based on the Cartesian cut cell mesh, here a cell-central finite volume method is applied in numerical discretization. Therein, Roe's approximate Riemann solver is adopted to calculate the numerical flux on each edge of fluid cell, where fluid variables are reconstructed by using a piecewise linear upwind scheme, and then a least-square method as discussed by W. H. Wang and Y. Y. Wang [4] and Superbee limiter as shown by Qian et al. [5] are used to achieve variable gradients and control spurious oscillations, respectively. Besides, the flux on solid boundary can be achieved by means of exact Riemann discontinuous solution by referring to W. H. Wang and Y. Y. Wang [4]. Then dual-time stepping technique with artificial compressibility method is taken for time advancing. Finally, here an approximate

LU factorization (ALU) scheme as mentioned by Pan and Lomax [15] is applied to solve linear equations. The more details about the above numerical scheme can be further found from the study of W. H. Wang and Y. Y. Wang [4].

2.4. Interactive Fluid-Body Motion

Here for the water-entry model of free-falling wedge, a fully body-fluid coupled velocity method as discussed elsewhere [4, 13] is used to calculate the fluid-body motion.

Firstly, the new body velocity can be obtained by

$$\left(v_S^{n+1}\right)^{k+1} = \omega\left(v_S^n + \frac{\Delta t F_{\text{body}}^k}{m}\right) + (1-\omega)\left(v_S^{n+1}\right)^k, \tag{2.5}$$

where Δt is the physical time interval, m is the mass of wedge, v_S^n is the vertical body velocity at the physical time n, and ω is a relaxation parameter to control the stability of subiteration. The larger the ω is, the faster the convergence rate of subiteration is.

As shown in (2.5), a subiterative process should be carried out at each physical moment, and the convergence standard is $(v_S^{n+1})^{k+1} - (v_S^{n+1})^k < 10^{-3}$. Then the final convergent $(v_S^{n+1})^{k+1}$ can be taken as the new velocity boundary condition v_S^{n+1} for the next physical time step $n+1$.

Subsequently, by using the calculated v_S^{n+1}, the new vertical displacement of solid body can be achieved by

$$y_S^{n+1} = \frac{\Delta t\left(v_S^n + v_S^{n+1}\right)}{2}, \tag{2.6}$$

where y_S^{n+1} is the new displacement condition of solid body for the next physical time step $n+1$.

3. Theory of Mechanical Energy Transport in Fluid Field

3.1. The Equation of Mechanical Energy

In order to be convenient for describing the equation of mechanical energy, here (2.2) and (2.3) should be rewritten in vector form firstly:

$$\frac{\partial(\rho\mathbf{v})}{\partial t} = -\left[\nabla\cdot\rho\mathbf{v}\mathbf{v}\right] - \nabla p + \rho\mathbf{B}, \tag{3.1}$$

where $\mathbf{v} = u\mathbf{i} + v\mathbf{j}$ is the fluid velocity, $\mathbf{B} = B_x\mathbf{i} + B_y\mathbf{j}$ is the fluid acceleration of body force, and $\nabla p = \partial p/\partial x\mathbf{i} + \partial p/\partial y\mathbf{j}$ is the gradient of fluid pressure.

Then by taking the dot product of fluid velocity vector $\mathbf{v}$ with (3.1), the final result is the equation of change for kinetic energy as discussed by Bird et al. [14]:

$$\frac{\partial}{\partial t}\left(\frac{1}{2}\rho v^2\right) = -\left(\nabla \cdot \left(\frac{1}{2}\rho v^2\right)\mathbf{v}\right) - (\nabla p \cdot \mathbf{v}) + \rho(\mathbf{v} \cdot \mathbf{B}). \tag{3.2}$$

In this equation, $\partial(\rho v^2/2)/\partial t$ is increase rate of kinetic energy per unit volume, $-(\nabla p \cdot \mathbf{v})$ is rate of work done by pressure of surroundings on the fluid, $-(\nabla \cdot (\rho v^2/2)\mathbf{v})$ is the rate of kinetic energy addition by convective transport, and $\rho(\mathbf{v} \cdot \mathbf{B})$ is rate of work done by body-fluid force.

With the introduction of the potential energy, (3.2) assumes the following form, and the equations of change for mechanical and potential energy can be written as

$$\frac{\partial}{\partial t}\left(\frac{1}{2}\rho v^2 + \rho g y\right) = -\left(\nabla \cdot \left(\frac{1}{2}\rho v^2 + \rho g y\right)\mathbf{v}\right) - (\nabla p \cdot \mathbf{v}), \tag{3.3}$$

$$\frac{\partial}{\partial t}(\rho g y) = -(\nabla \cdot (\rho g y)\mathbf{v}) - \rho(\mathbf{v} \cdot \mathbf{B}), \tag{3.4}$$

where $\partial(\rho g y)/\partial t$ is the increase rate of potential energy per unit volume, and $-(\nabla \cdot (\rho g y)\mathbf{v})$ is the rate of potential energy addition per unit volume by convective transport.

3.2. The Macroscopic Balance of Mechanical Energy in Fluid Field

The most important use of microscopic kinetic plus potential energy (3.3) is for the development of the macroscopic mechanical energy balance, which can be integrated in whole fluid field:

$$\int_{V(t)} \frac{\partial}{\partial t}\left(\frac{1}{2}\rho v^2 + \rho g y\right) dV = -\int_{V(t)} \left[\nabla \cdot \left(\frac{1}{2}\rho v^2 + \rho g y\right)\mathbf{v}\right] dV - \int_{V(t)} (\nabla p \cdot v) dV. \tag{3.5}$$

Next based on the Leibniz equation and Gauss law as shown by Bird et al. [14], (3.5) can be rewritten as

$$\frac{d}{dt}\int_{V(t)} \left(\frac{1}{2}\rho v^2 + \rho g y\right) dV = -\int_{S(t)} \left[\mathbf{n} \cdot \left(\frac{1}{2}\rho v^2 + \rho g y\right)(\mathbf{v} - \mathbf{v_B})\right] dS - \int_{S(t)} (\mathbf{n} \cdot p\mathbf{v}) dS, \tag{3.6}$$

where $\mathbf{v_B}$ represents the boundary velocity of fluid field.

4. Results of Test Case and Discussions

4.1. Verification of the Present Numerical Method

In this section, two kinds of water-entry models of 2D free-falling wedge are created and numerically simulated to validate the present method by comparing the calculated results with experimental data of Zhao and Faltinsen [1] and Sun et al. [2].

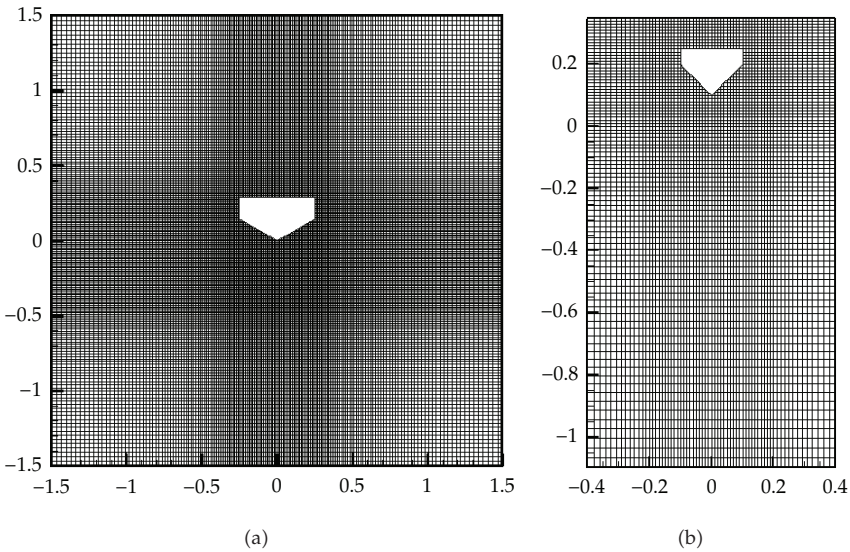

Figure 1: Global mesh of test model 1 (a) and test model 2 (b) in fluid field.

The first test model was created on a square domain of 3 m×3 m half occupied by water and half by air, and the wedge with 30° was 0.5 m wide, 0.29 m high, and 241 kg weight. The zero time ($t = 0$) of this case was selected as the moment that the apex of wedge contacts the initial calm free surface. Here for the comparison with experimental data as described by Zhao and Faltinsen [1], the initial velocity of wedge was prescribed as −6.15 m/s. On the other hand, for the second test model, the computational domain was a square of 0.8 m × 1.45 m, and the water depth was 1.1 m. Furthermore, the wedge with 45° was 0.6 m long, 0.2 m wide, and 7.787 kg weight. The zero physical time ($t = 0$) was the moment that the apex of wedge is 0.1 m up from the initial free surface, and then the wedge begun to fall freely.

In numerical calculation, the physical time Δt was 0.0001 s, the fictitious time $\Delta\tau$ was 0.01 s, the artificial compressibility coefficient β was 500, ω was taken as 0.8, and the gravity acceleration was 9.81 m/s^2.

Furthermore near solid boundary, the local meshes with equal spacing $\Delta x = \Delta y =$ 0.01 m were refined and regular, and then the mesh size gradually enlarged away from boundary. Thus, the inhomogeneous meshes (180 × 190 for model 1 and 66 × 90 for model 2) were generated in fluid field as shown in Figure 1.

In Figure 2, the time histories of hydrodynamic and acceleration versus numerical results and experiment are described and compared, F_h is the hydrodynamic on wedge, a is the acceleration of wedge, and t is the physical time. From the figure, it can be found that the numerical results of the present method are in good agreement with the experimental data of Zhao and Faltinsen [1] and Sun et al. [2]. Furthermore, it should be noted that there is a little difference about peak value in acceleration curve of Figure 2(b), which may be caused by the decrease of wedge velocity on the initial water-entry moment due to the resistance of experimental equipment.

Thus, the present method in this paper can be verified to be available and feasible for the study of free-falling wedge during water-entry phase. Furthermore, in order to make a long-time analysis on the energy transport and control the reflection of left and right

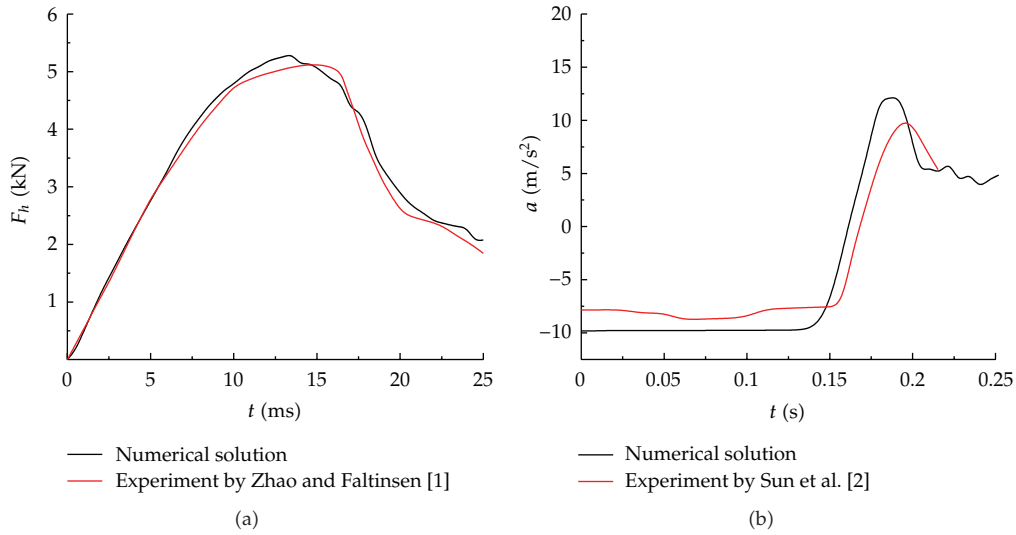

Figure 2: Comparison between numerical solutions of hydrodynamic (a); wedge acceleration (b) and experiment data of Zhao and Faltinsen [1] and Sun et al. [2].

boundaries, based on the test model 2, the width of computational domain is broaden from 0.8 m to 1.65 m in the following numerical simulation.

4.2. Macroscopic Energy Conversion of Overall Wedge-Fluid System

4.2.1. Change of Mechanical Energy for Free-Falling Wedge

At the initial moment, the wedge is 0.1 m up from the calm free surface and then begins to fall freely. During the whole motion process, the total mechanical energy (kinetic and potential energy) of wedge continuously changes as follows:

$$\begin{aligned} \frac{d}{dt}\left(\frac{1}{2}m{v_S}^2 + mgy_S\right) &= \mathbf{F}_h \cdot \mathbf{v_S}, \\ \frac{d}{dt}\left(\frac{1}{2}m{v_S}^2\right) &= m\mathbf{g} \cdot \mathbf{v_S} + \mathbf{F}_h \cdot \mathbf{v_S}, \\ \frac{d}{dt}(mgy_S) &= -m\mathbf{g} \cdot \mathbf{v_S}, \end{aligned} \tag{4.1}$$

where y_S is the vertical coordinate of wedge center, $\mathbf{v_S} = v_S\mathbf{j}$ is the velocity vector of wedge, $\mathbf{F}_h$ is the hydrodynamic on wedge, $\mathbf{g} = g\mathbf{j}$ is the vector of gravity acceleration, $mv_S{}^2/2$ is the kinetic energy of wedge, and mgy_S is the potential energy of wedge (here $y = 0$ is selected as zero position of potential energy).

In Figure 3, the time histories of variation rate for total mechanical energy, hydrodynamic and velocity of free-falling wedge are shown, dE/dt is the variation rate of total energy, and v_S is the body velocity. From the figure, it can be found that based on the movement characteristic of wedge at various time intervals, the whole motion process can be classified into three phases. Firstly, before the wedge impacts water surface, the hydrodynamic on

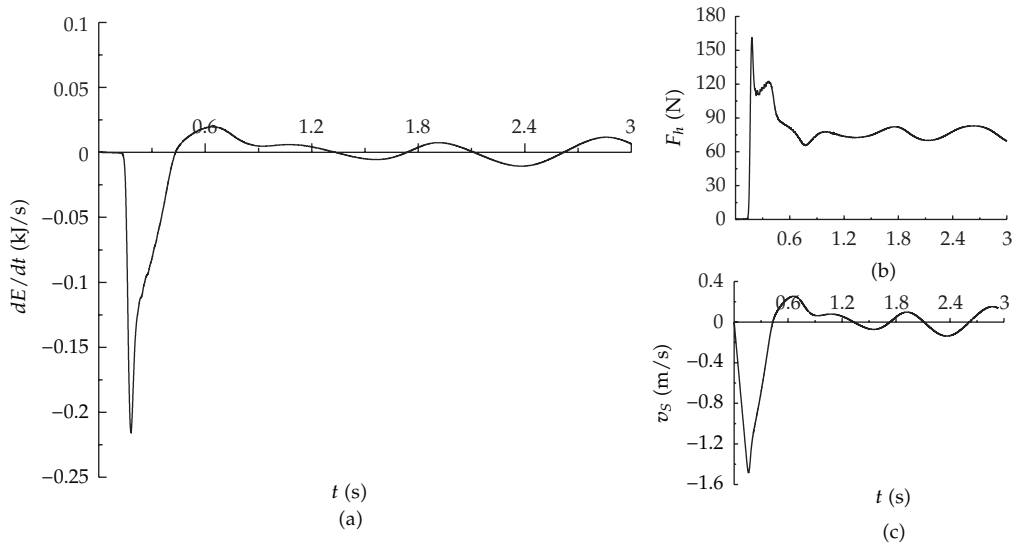

Figure 3: Time histories of variation rate for total energy (a), hydrodynamic (b), and velocity (c) of free-falling wedge.

wedge is very small and can be neglected. Thus, wedge keeps accelerating downward in air. Meanwhile, the total mechanical energy of wedge basically remains unchanged. Secondly, wedge affects free surface and then enters water. On this time interval, the hydrodynamic on solid boundary suddenly and rapidly heightens, which cause the wedge to reduce the speed. Hence, the mechanical energy of wedge gradually decrease and transfer to fluid field. As the wedge further travels in water, by hydrodynamic on wedge, the body velocity becomes less and less. Thirdly, until time advances to about 0.43 s, the velocity of wedge reduces to zero and will become opposite direction. From then on, the wedge moves up and down with small amplitude, which causes the mechanical energy of overall system to alternately convert between wedge and fluid field.

Here time histories of accumulative variation of energy and its ratio for free-falling wedge are shown in the Figure 4, dE is the accumulative variation of energy, work done by fluid is the accumulative energy transport from wedge to fluid field. The energy conversion of wedge during the whole motion process can be well described in this figure. For the first phase of wedge moving in air, the potential energy of wedge becomes basically kinetic energy of body. Then in the second stage of initial water-entry, the decrease of potential is equal to the sum of kinetic energy addition of wedge and increase of fluid energy. Finally, in the third time interval the wedge moves up and down. From the figure, it can be found that the kinetic energy of wedge tends to zero, and the potential energy of wedge and fluid energy can change each other. Therefore, it can be concluded that during the water-entry phase the variation of potential energy of free-falling wedge is the essential source of energy transport of overall system.

4.2.2. Macroscopic Energy Transport for Whole Fluid Field

In order to study the macroscopic energy transport of fluid field, here based on (3.6) the various boundaries of fluid field for water-entry model should be discussed firstly.

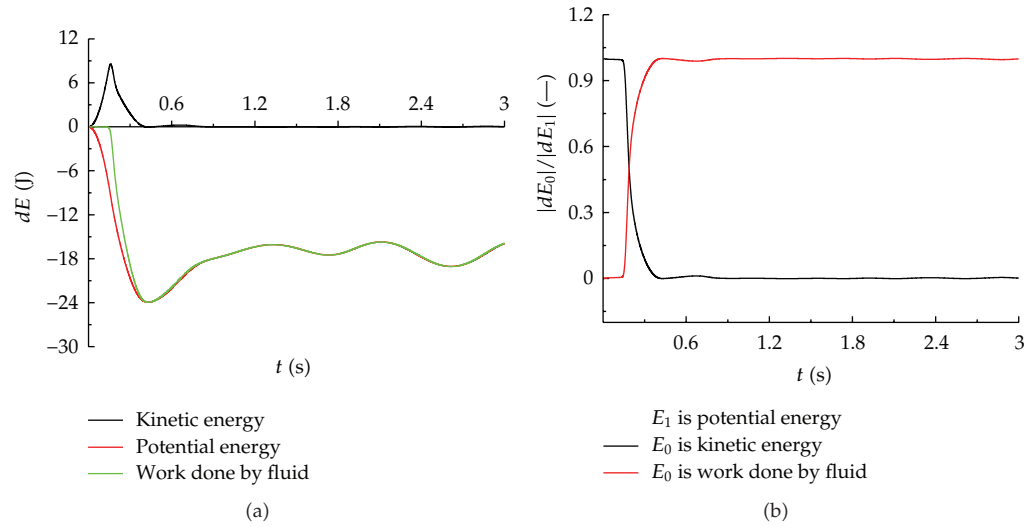

Figure 4: Time histories of accumulative variation of energy (a) and its ratio (b) for free-falling wedge.

For the computation domain, up edge is open and outlet boundary, solid edges of wedge are moving wall boundary, and left, down, and right edges are fixed wall boundary. Thus, on the up boundary $v_B = 0$, on the solid boundaries of wedge $\mathbf{n} \cdot \mathbf{v} = \mathbf{n} \cdot \mathbf{v_S} \neq 0$, and on the fixed boundary (left, down, and right edges) $\mathbf{n} \cdot \mathbf{v} = \mathbf{n} \cdot \mathbf{v_B} = 0$ should be used. On this basis, (3.6) related to water-entry model can be simplified as

$$\frac{d}{dt}\int_{V(t)}\left(\frac{1}{2}\rho v^2 + \rho g y\right)dV = -\int_{\text{up}}\left[\mathbf{n}\cdot\left(\frac{1}{2}\rho v^2 + \rho g y\right)\mathbf{v}\right]dS - \int_{\text{up}}(\mathbf{n}\cdot p\mathbf{v})dS - \int_{\text{rigid}}(\mathbf{n}\cdot p\mathbf{v_S})dS. \tag{4.2}$$

In this equation, $d[\int_{V(t)}(\rho v^2/2 + \rho g y)dV]/dt$ is the increase rate of kinetic plus potential energy in fluid field, $-\int_{\text{up}}[\mathbf{n}\cdot(\rho v^2/2 + \rho g y)\mathbf{v}]dS$ is the rate of kinetic and potential energy addition of fluid field from up boundary by convection, $-\int_{\text{up}}(\mathbf{n}\cdot p\mathbf{v})dS$ is the rate of work done by pressure on up boundary, and $-\int_{\text{rigid}}(\mathbf{n}\cdot p\mathbf{v_S})dS$ is the rate of work done by pressure on solid boundary of wedge.

Based on the Helmholtz velocity decomposing theorem, the fluid velocity can be written as

$$V_x = V_{xO} + \varepsilon_x dx + \gamma dy - \omega dy, \tag{4.3}$$

$$V_y = V_{yO} + \varepsilon_y dy + \gamma dx + \omega dx, \tag{4.4}$$

where V_{xO} and V_{yO} are the x- and y-translational fluid velocities versus point O, $\varepsilon_x = \partial V_x/\partial x$ and $\varepsilon_y = \partial V_y/\partial y$ are x and y-linear deforming velocities of fluid, $\gamma = (\partial V_x/\partial y + \partial V_y/\partial x)/2$ is the shearing deformation velocity of fluid, $\omega = (\partial V_y/\partial x - \partial V_x/\partial y)/2$ is the rotation angular velocity around point O, and $\mathbf{r} = dx\mathbf{i} + dy\mathbf{j}$ is the position vector to point O.

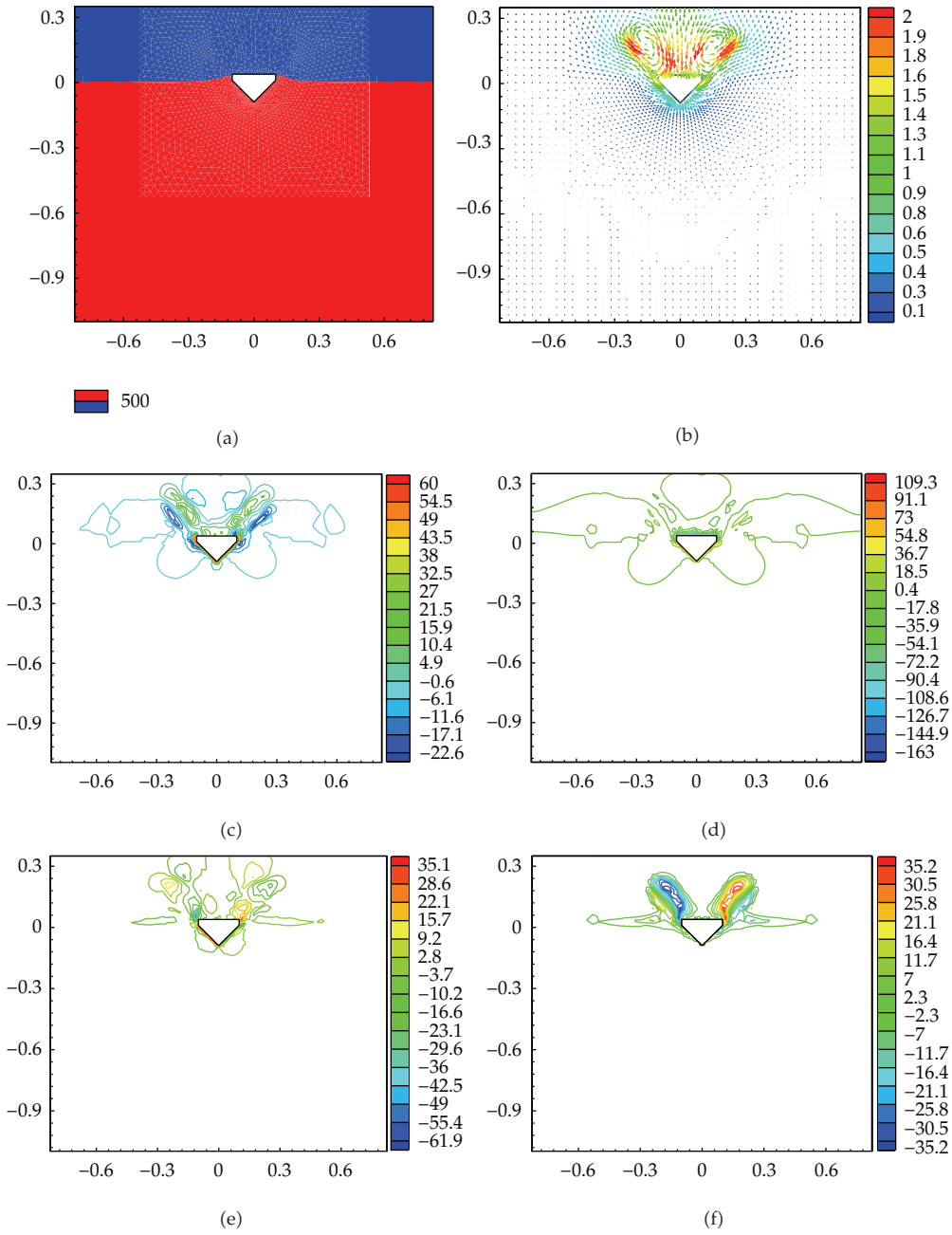

Figure 5: Information of fluid motion at the moment of 0.21 s. (a) free surface; (b) velocity vector; (c) x- and (d) y-linear-deforming velocities; (e) shearing deformation velocity; (f) rotation angular velocity.

In order to accurately and reasonably calculate the $d[\int_{V(t)}(\rho v^2/2 + \rho g y)dV]/dt$, here the fluid motion for water-entry model of free-falling wedge should be discussed.

In Figure 5, the free surface, velocity vector, x- and y-linear deforming, shearing deformation, and rotation angular velocity at the moment of 0.21 s are demonstrated. From

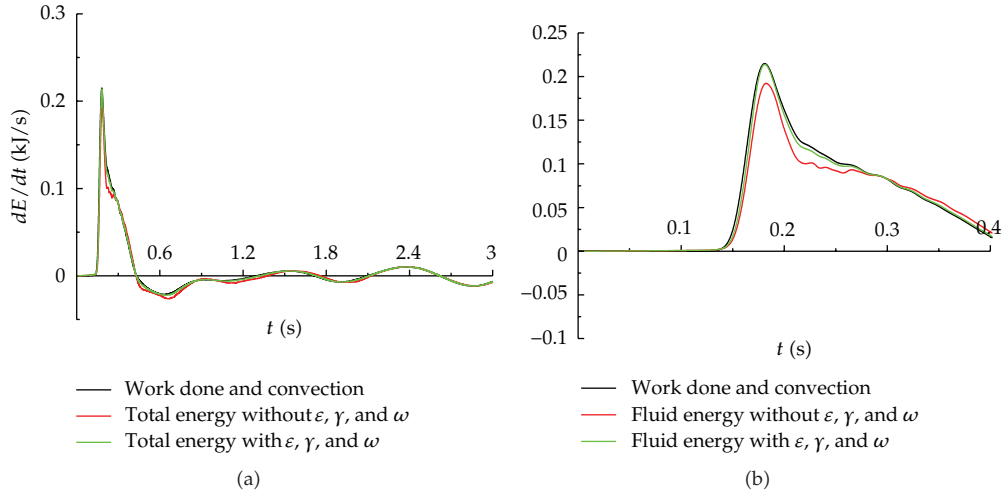

Figure 6: Time histories of numerical solutions for rate of work done and convection addition to fluid field and increase of fluid energy without or with consideration of ε, γ and ω during the whole and initial water-entry phase.

this figure, it can be found that for the water-entry model with air and water, the fluid is not only rotational motion, but also includes linear and shearing deformation.

Besides, Figure 6 shows the time histories of numerical solutions for rate of work done and convection in addition to fluid field and increase of fluid energy without or with consideration of ε, γ and ω during the whole and initial water-entry phase, ε_x and ε_y are x and y-linear deforming, γ is the shearing deformation, and ω is rotation angular velocity. As shown in this figure, the results shows that in the calculation of fluid energy by finite volume method for the water-entry model with both water and air, neglecting the influence of ε, γ, and ω may produce numerical error. Thus in order to more accurately predict the energy variation of entire fluid filed, fluid rotational motion and deformation should be taken into account in the numerical FVM method.

In Figure 7, time histories of accumulative variation of energy and its ratio in fluid field are demonstrated, and the increase of total energy in fluid field comes from the work done and convection on boundaries. Here the accumulative variation of energy and its ratio are also analyzed in three time intervals. In the first stage, the wedge has not yet entered water. It can be found that the potential energy in fluid field still remain unchanged from the figure. Next for the second phase, the wedge moves through water surface. Increase of total energy all become kinetic and potential energy in fluid field. Finally, in the third time interval, with the time advancing the wedge moves up and down, which cause the ratio of kinetic and potential to total energy to have a little oscillation around 25% and 75%, respectively.

Moreover, it should be noted that in the third phase the variation of fluid energy is repeated plus-minus oscillation, so in order to clearly and definitely discuss and analyze the transport phenomena of fluid energy for water-entry model of free-falling wedge, in the following study the calculation time range is selected from 0–0.4 s, which is the time interval of fluid energy monotonously increasing.

Figure 8 demonstrates time histories versus ratio (a) and rate (b) of energy variation in fluid field during the initial water-entry moment. From Figure 8(a), it can be obtained that the ratio of work done by wedge to increase fluid energy is approximately equal to 1.0, which

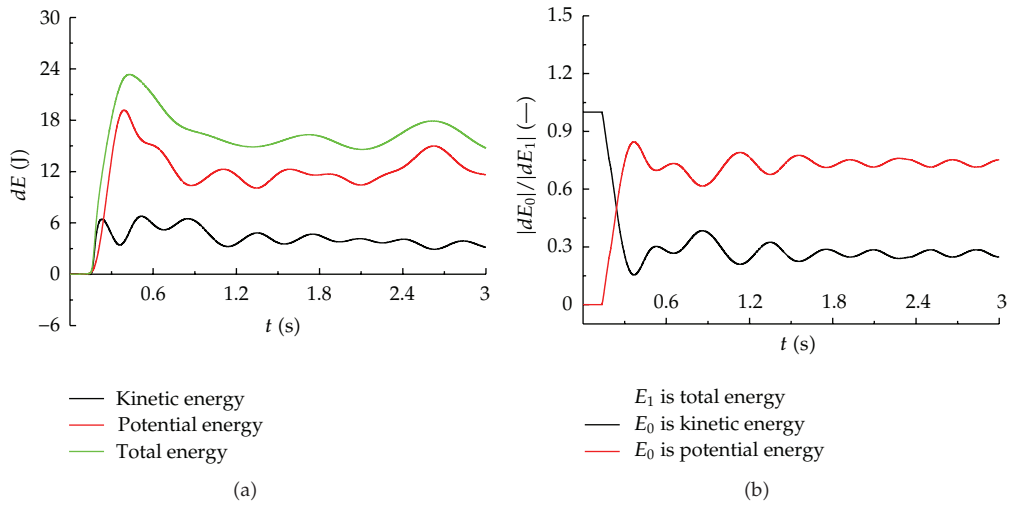

Figure 7: Time histories of accumulative variation of energy (a) and its ratio (b) in fluid field.

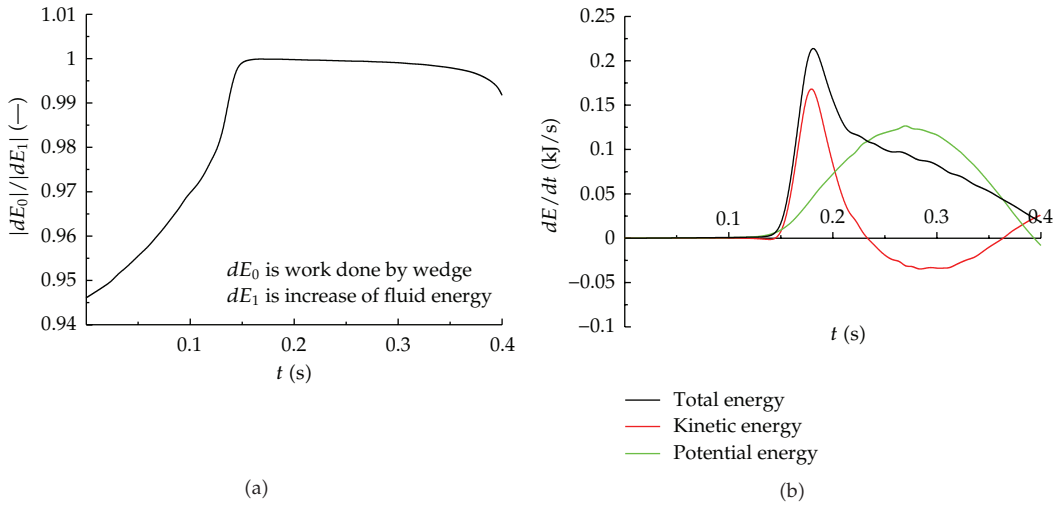

Figure 8: Time histories versus ratio (a) and rate (b) of energy variation in fluid field during the initial water-entry moment.

shows that work done by wedge is the main origin and reason for the change and transport of fluid energy.

Furthermore, the variation rates versus kinetic, potential and total energy are drawn in Figure 8(b), which can describe the transport phenomena of fluid energy by combining with fluid motion. During the time interval of wedge moving in air, the hydrodynamic on wedge is very small, so the rates of kinetic, potential, and total energy in fluid field are minute and approximate to zero. In the initial phase of water-entry, impulse hydrodynamic with high-pressure peaks on wedge causes fluid particle near solid boundary to accelerate and free surface to rise up, which will result in the rapid increase of kinetic and steadily enhancement of potential energy. As the wedge pieces through free surface, the pressuring effect of wedge on fluid reduces, and the rate of kinetic energy in fluid field gradually decreases. With

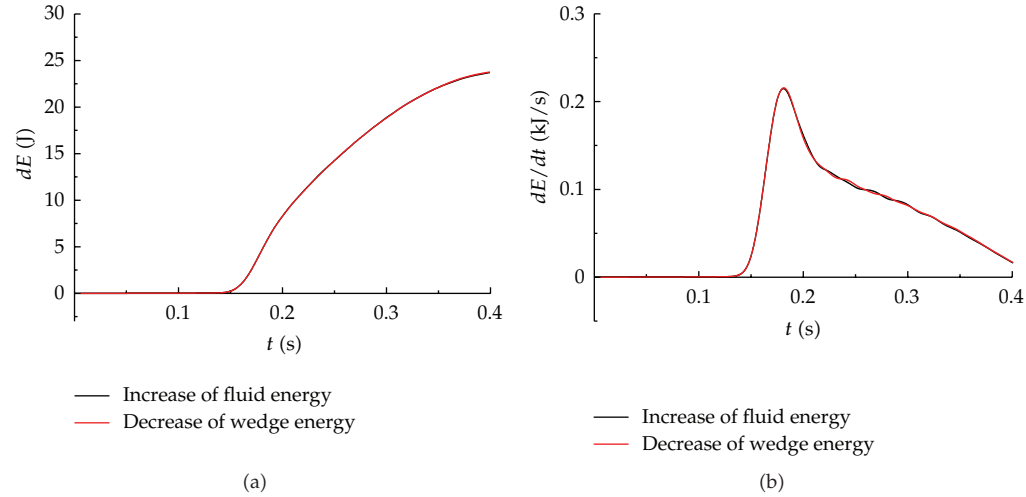

Figure 9: Comparison of value and its rate versus increase of fluid energy and decrease of wedge energy during the initial water-entry phase.

physical time advancing, due to the further reduction of fluid pressure and decelerating effect of gravity, the rate of kinetic energy becomes negative. However, at this moment the global direction of fluid velocity near free surface is still upward, which cause the potential energy to continuously heighten. As the wedge further travels into water, for the sake of gravity, the fluid near free surface ultimately will fall down, the rate of potential energy in fluid field will be negative, and meanwhile the kinetic energy will accordingly improve.

4.2.3. Validity of Energy Conservation of Overall Body-Fluid System

The increase and its rate of fluid energy and decrease of wedge energy are compared in Figure 9. From the figure, it is obvious that both variations of fluid and wedge energy are almost the same, and a very little difference may be caused by the minute work done or convection on up boundary. Therefore, it can be concluded that energy conservation of overall system can be satisfied in current numerical method.

4.3. Microscopic Energy Transformation in Fluid Field

In this section, for further and better studying how fluid energy changes and transports, some microscopic details in fluid field (such as velocity vector, pressure gradient, and distribution of transient variation for kinetic and potential energy) are discussed at three classic moments (t = 0.06, 0.18, and 0.27 s), which are chosen from Figure 8.

At t = 0.06 s, the wedge has not contacted and affected free surface yet, and the information about the change of fluid energy in air can be described and studied as in Figure 10 .

In Figure 10, microscopic details of fluid energy at t = 0.06 s are described. Firstly based on (3.2) and (3.4), various influential factors on the change of fluid energy are shown in Figures 10(c)–10(j), respectively, which are successively the convective transport of kinetic energy $-(\nabla \cdot (\rho v^2/2)\mathbf{v})$, convective vector of kinetic energy (from high to low) $-\nabla \cdot (\rho v^2/2)$,

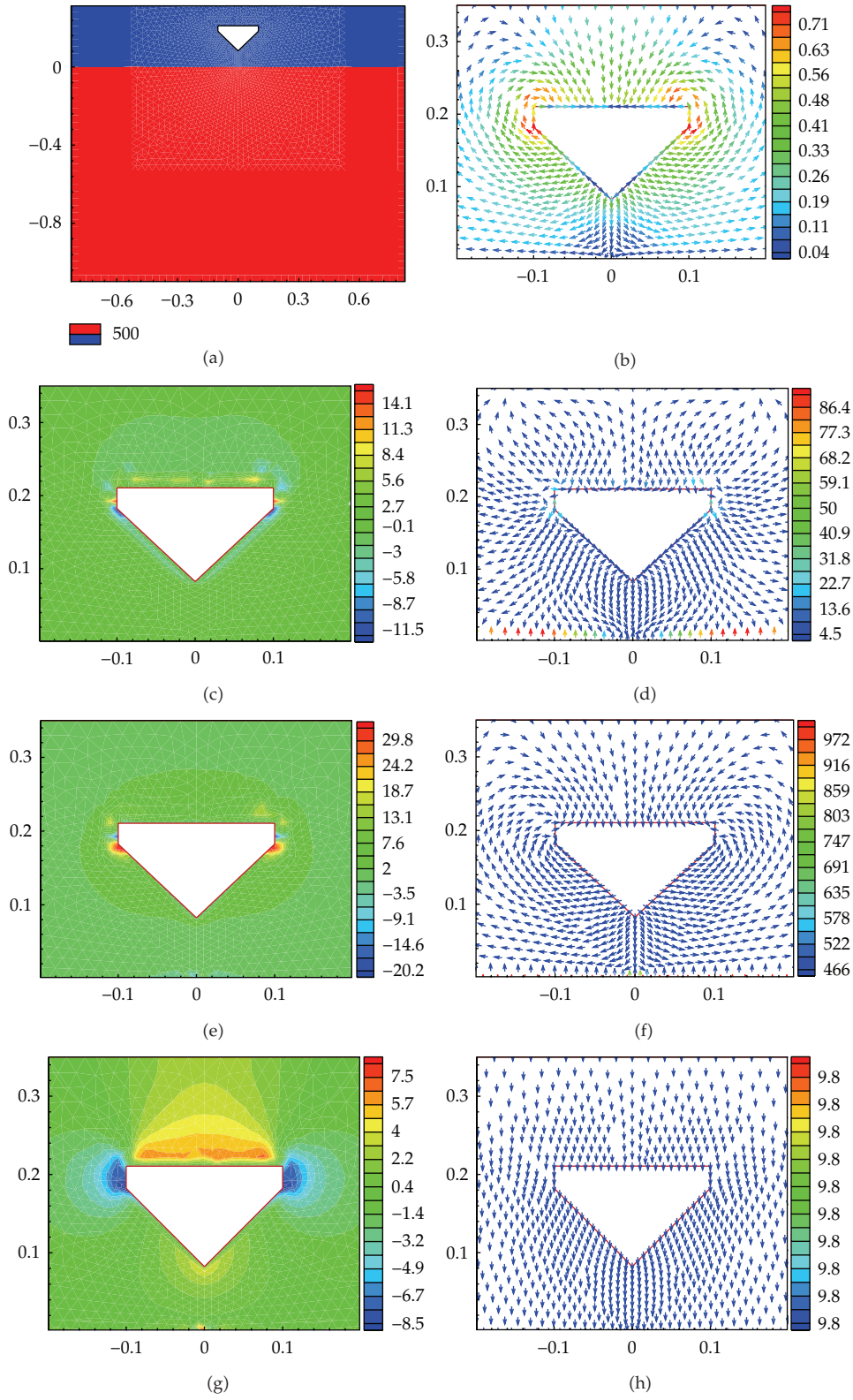

Figure 10: Continued.

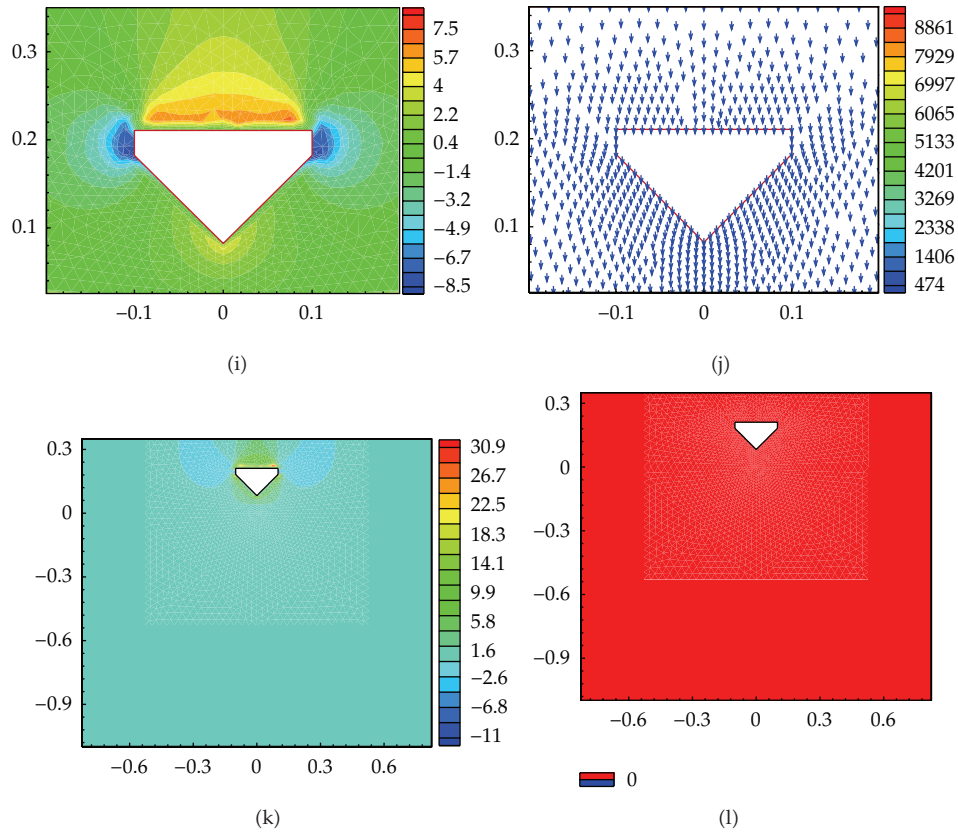

Figure 10: Microscopic details of fluid energy at $t = 0.06$ s. (a) free surface profile; (b) velocity vector; (c) convection of kinetic energy; (d) convective vector of kinetic energy (high to low); (e) work done by pressure; (f) convective vector of pressure; (g) work done by gravity; (h) gravity vector; (i) convection of potential energy; (j) convective vector of potential energy; (k) transient change of kinetic energy; (l) transient change of potential energy.

work done by pressure $-(\nabla p \cdot \mathbf{v})$, convective vector of pressure $-\nabla p$, work done by gravity $\rho(\mathbf{v} \cdot \mathbf{B})$, gravity vector $\mathbf{B}$, convection of potential energy $-(\nabla \cdot (\rho g y)\mathbf{v})$, and convective vector of potential energy $-\nabla \cdot (\rho g y)$. From the figure, it can be found that the effect of these above-mentioned factors on change of fluid energy is related to the direction and value of fluid velocity. Now take Figures 10(e) and 10(f) for example, and Figure 10(f) shows the convective direction of fluid pressure (from high to low). By comparing convective vector of pressure with the velocity vector of Figure 10(b), it is obvious that the directions versus the above two kinds of vectors are the same in most areas, except a small local zone near both straight edges of wedge, which results in the regional distribution about the increase or decrease of fluid energy in Figure 10(e). Besides as shown in Figure 10(b), the fluid velocities are up to maximum on the both corners of wedge. Thus in Figure 10(e), there are two deep red zones with highest rate of energy addition by work done by pressure on the corners of wedge according to fluid velocity. By synthetically analyzing all influential factors, the transient changes of kinetic energy $\partial(\rho v^2/2)/\partial t$ and potential energy $\partial(\rho g y)/\partial t$ can be described in Figures 10(k) and 10(l). From the figure, because the convection of potential energy and work done by gravity is almost the same, the potential energy will remain unchanged as shown

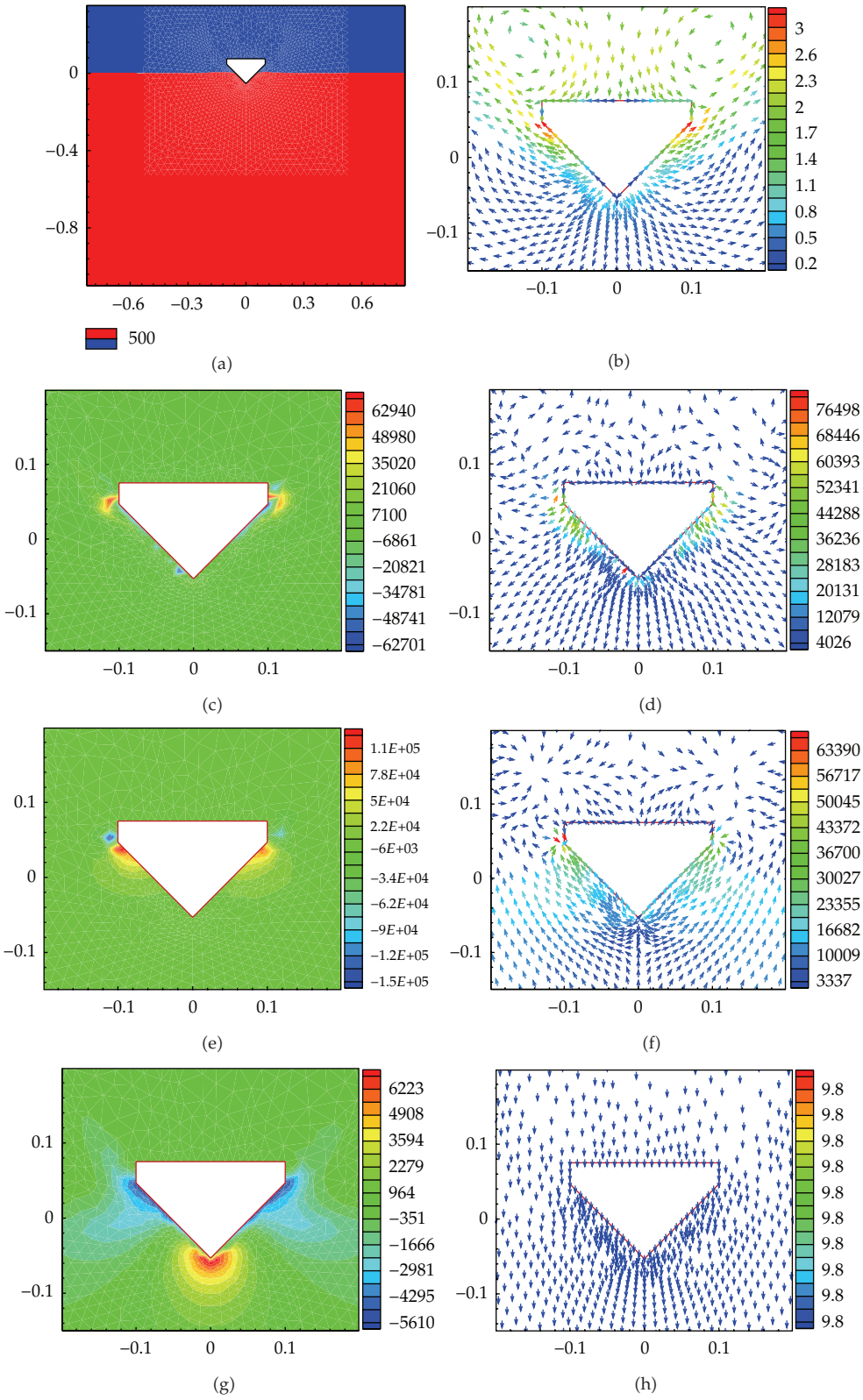

Figure 11: Continued.

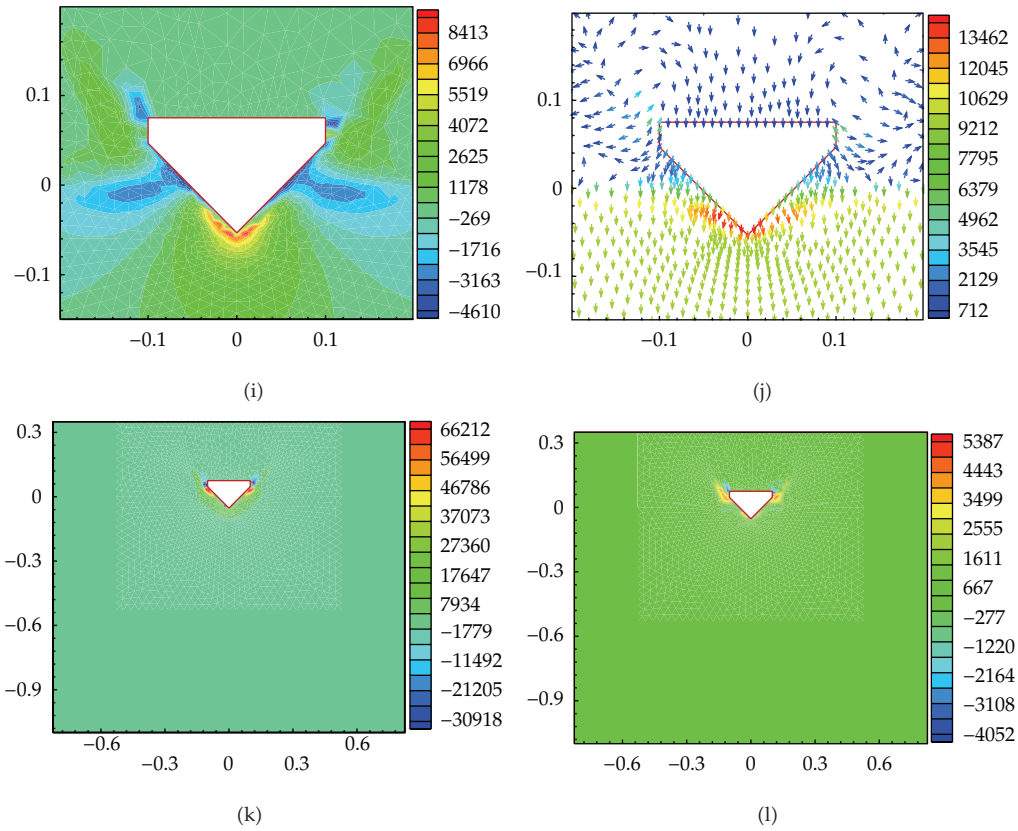

Figure 11: Microscopic details of fluid energy at $t = 0.18$ s. (a) free surface profile; (b) velocity vector; (c) convection of kinetic energy; (d) convective vector of kinetic energy (high to low); (e) work done by pressure; (f) convective vector of pressure; (g) work done by gravity; (h) gravity vector; (i) convection of potential energy; (j) convective vector of potential energy; (k) transient change of kinetic energy; (l) transient change of potential energy.

in Figure 10(l). On the other hand, due to the influence of convective transport and work done by pressure and gravity, the kinetic energy will vary just near the solid boundary of wedge. Furthermore, only in very minute area on the both straight edges of wedge, the color of Figure 10(k) is deep blue, where the kinetic energy of fluid field will most quickly reduce. But in other zones near wedge the kinetic energy will more or less increase.

Figure 11 demonstrates microscopic information of fluid energy at $t = 0.18$ s. From Figures 11(a) and 11(b), it can be found that on this moment the wedge is piercing the free surface, and water rises up along the slope edges, and the displacement waves are formed. Meanwhile, the air between the body and free surface escapes and separates at the corner of wedge to form a pair of symmetric vortices. All influential effects on the change of fluid energy are shown in Figures 11(c)–11(j), respectively and then studied to achieve the distribution of transient changes of kinetic and potential energy as shown in Figures 11(k) and 11(l). At $t = 0.18$ s, the wedge has entered water and forces free surface to rise upward, which results in the increase of potential energy along both slope edges of wedge in Figure 11(l). Furthermore, according to the convection and work done in Figures 11(c), 11(e), and 11(g), it can be obtained that the work done of pressure is main reason of energy variation

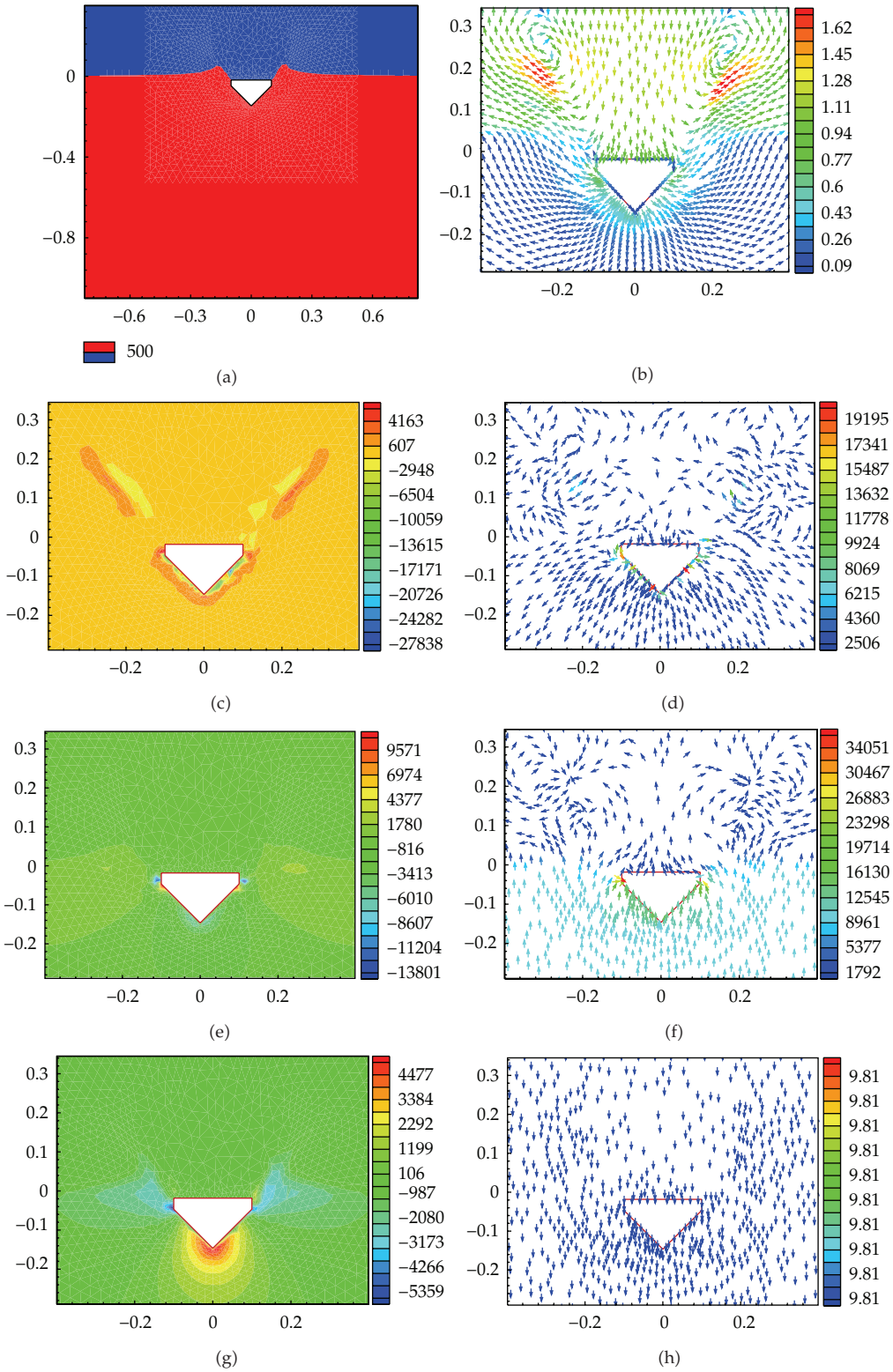

Figure 12: Continued.

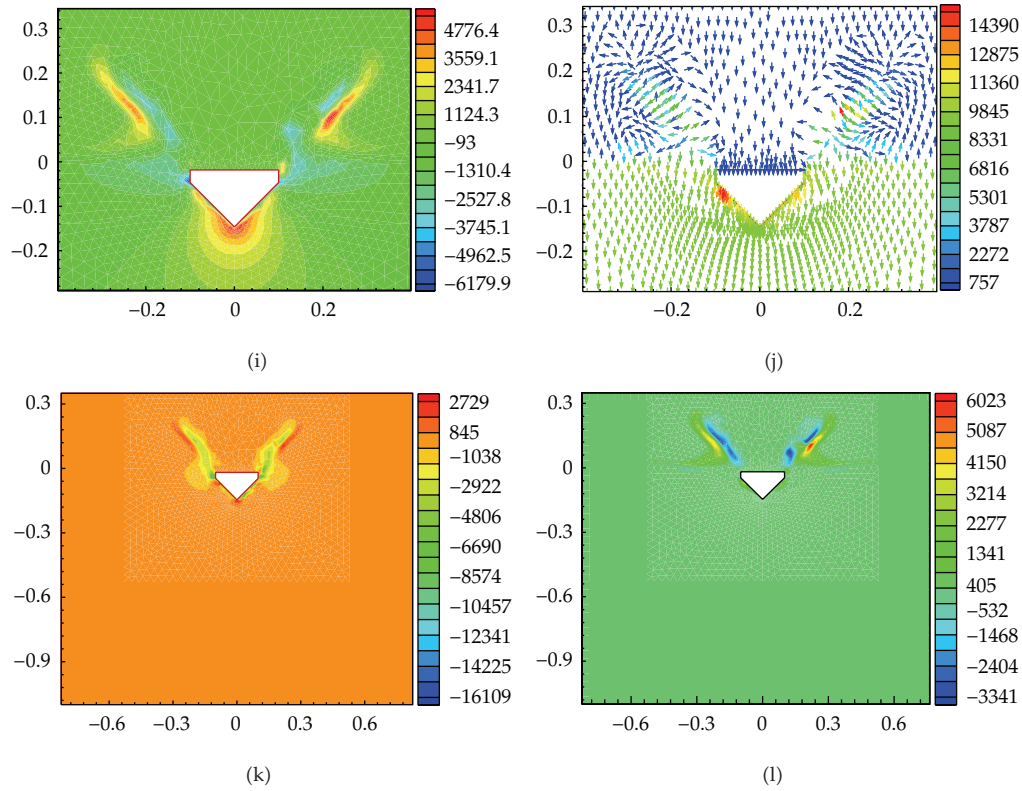

Figure 12: Microscopic details of fluid energy at $t = 0.27$ s. (a) free surface profile; (b) velocity vector; (c) convection of kinetic energy; (d) convective vector of kinetic energy (high to low); (e) work done by pressure; (f) convective vector of pressure; (g) work done by gravity; (h) gravity vector; (i) convection of potential energy; (j) convective vector of potential energy; (k) transient change of kinetic energy; (l) transient change of potential energy.

for kinetic energy. In Figure 11(f), due to the motion characteristic of free-falling wedge at $t = 0.18$ s, there are two prominent low-pressure zones at both corners of wedge, which cause remarkable increase on both slope edges and great decrease on both straight edges for the work done by pressure and kinetic energy versus Figures 11(e) and 11(k), respectively.

The fluid details about kinetic and potential energy at $t = 0.27$ s are drawn in Figure 12. At this time, the two intersections between wedge and free surface have been to the highest point of both straight sides, and the two air vortices are far away from wedge. In the same way, various influential effects on the variation of fluid energy can be achieved in Figures 12(c)–12(j), and on this basis the distribution of transient transformation of kinetic and potential energy are demonstrated in Figures 12(k) and 12(l). As shown in these figures, the present location and movement trend of free surface determine the color distribution of transient change for kinetic and potential energy, that is, the zone with yellow-green color in Figure 12(k) or blue color of Figure 12(l) represents the present location of free surface which will move toward the area with red color in Figure 12(k) or red-yellow color of Figure 12(l). Furthermore, by analyzing the difference of value among various contours, it can be found that at this moment the free surface will move up and outwards with less and less velocity, which causes the increase of potential energy and decrease of kinetic energy.

Finally by synthetically analyzing Figures 10–12, it can be concluded that in fluid field the variation of kinetic and potential energy just locally takes place near wedge and free surface. Furthermore, by comparing Figures 10–12 with each other, the rate of variation for kinetic and potential energy at $t = 0.06$ s is relatively minute. Next, at $t = 0.18$ s, the kinetic and potential energy present a fast growth tendency, and the rate of variation for kinetic energy is relatively maximum. Finally, on the moment of $t = 0.27$ s, the rate of potential energy is positive and relatively maximum, but the kinetic energy in fluid field globally appears to be a downward trend. Thus, the microscopic information of fluid energy in Figures 10, 11, and 12 can well verify and support the macroscopic variation trend of kinetic and potential energy of fluid field in Figure 8.

5. Conclusions

In this paper, a free surface capturing method and Cartesian cut cell mesh are used to numerically simulate the water-entry model of free-falling wedge. By means of the calculated results, the physical phenomena and mechanical energy transports of body-fluid interactive system are studied from macroscopic energy conversion of overall body-fluid system and microscopic energy transformation in fluid field. Finally some useful conclusions can be made as follows:

(1) by the present method of this paper, energy conservation is always satisfied in the whole phase of numerical calculation;

(2) for water-entry model of free-falling wedge with both air and water, the fluid motion includes not only rotation angular velocity but also linear and shearing deformation, which will have an influence on the numerical calculation of fluid energy by finite volume method and should be taken into account;

(3) during the initial phase of water-entry, for the overall system the variation of potential energy of free-falling wedge is the essential source of energy transport, which should change the kinetic energy of wedge, kinetic energy, and potential energy of fluid;

(4) during the initial phase of water-entry of free-falling wedge, compared with the work done by wedge, the energy transport from open boundary can be neglected for the variation of fluid energy. Furthermore, the gradient of fluid pressure caused by wedge is the basic and original cause of fluid motion and energy transport in fluid field;

(5) during the initial phase of water-entry of free-falling wedge, the change regularities of kinetic and potential energy in fluid field are studied and successfully associated with the fluid motion.

Furthermore, in the future research other water-entry problems (such as water-entry with constant velocity and water-entry of elastic body) should be studied and analyzed.

References

[1] R. Zhao and O. M. Faltinsen, "Water entry of arbitrary two-dimensional sections with and without flow separation," in *Twenty-first Symposium. On Naval Hydrodynamics*, National Academy, Washington, DC, USA, 1997.

[2] H. Sun, Z. H. Lu, and Y. S. He, "Experimental research on the fluid-structure interaction in water entry of 2D elastic wedge," *Journal of Hydrodynamics*, vol. 18, no. 1, pp. 104–109, 2003.
[3] T. Bunnik and B. Buchner, "Numerical prediction of wave loads on subsea structures in the splash zone," in *Proceedings of the 14th International Offshore and Polar Engineering Conference*, pp. 284–290, Toulon, France, 2004.
[4] W. H. Wang and Y. Y. Wang, "An improved free surface capturing method based on Cartesian cut cell mesh for water-entry and exit problems," *Proceedings of the Royal Society A*, vol. 465, no. 2106, pp. 1843–1868, 2009.
[5] L. Qian, D. M. Causon, D. M. Ingram et al., "A free-surface capturing method for two fluid flows with moving bodies," *Proceedings of the Royal Society A*, vol. 462, no. 2065, pp. 21–42, 2006.
[6] F. J. Kelecy and R. H. Pletcher, "The development of a free surface capturing approach for multidimensional free surface flows in closed containers," *Journal of Computational Physics*, vol. 138, no. 2, pp. 939–980, 1997.
[7] D. Pan and C. H. Chang, "The capturing of free surfaces in incompressible multi-fluid flows," *International Journal for Numerical Methods in Fluids*, vol. 33, no. 2, pp. 203–222, 2000.
[8] G. Yang, D. M. Causon, D. M. Ingram, R. Saunders, and P. Batten, "A Cartesian cut cell method for compressible flows. Part A. Static body problems," *Aeronautical Journal*, vol. 101, no. 1002, pp. 47–56, 1997.
[9] G. Yang, D. M. Causon, D. M. Ingram, R. Saunders, and P. Battent, "A Cartesian cut cell method for compressible flows. Part B. Moving body problems," *Aeronautical Journal*, vol. 101, no. 1002, pp. 57–65, 1997.
[10] D. M. Causon, D. M. Ingram, and C. G. Mingham, "A Cartesian cut cell method for shallow water flows with moving boundaries," *Advances in Water Resources*, vol. 24, no. 8, pp. 899–911, 2001.
[11] P. L. Roe, "Approximate Riemann solvers, parameter vectors, and difference schemes," *Journal of Computational Physics*, vol. 43, no. 2, pp. 357–372, 1981.
[12] W. Y. Soh and J. W. Goodrich, "Unsteady solution of incompressible Navier-Stokes equations," *Journal of Computational Physics*, vol. 79, no. 1, pp. 113–134, 1988.
[13] F. J. Kelecy and R. H. Pletcher, "The development of a free surface capturing approach for multidimensional free surface flows in closed containers," *Journal of Computational Physics*, vol. 138, no. 2, pp. 939–980, 1997.
[14] R. B. Bird, W. E. Stewart, and E. N. Lightfoot, *Transport Phenomena*, John Wiley & Sons, 2nd edition, 2001.
[15] D. Pan and H. Lomax, "A new approximate LU factorization scheme for the Reynolds-averaged Navier-Stokes equations," *American Institute of Aeronautics and Astronautics*, vol. 26, no. 2, pp. 163–171, 1988.